JOURNAL OF GEOPHYSICAL RESEARCH, VOL. 107, NO. D5, 4042, 10.1029/2001JD000601, 2002

Relationship between photolysis frequencies derived from spectroscopic measurements of actinic fluxes and irradiances during the IPMMI campaign

Richard McKenzie and Paul Johnston
National Institute of Water and Atmospheric Research, Lauder, Central Otago, New Zealand

Andreas Hofzumahaus and Alexander Kraus[1]
Institut für Chemie und Dynamik der Geosphäre, Institut II: Troposphäre, Forschungszentrum Jülich, Jülich, Germany

Sasha Madronich, Chris Cantrell, Jack Calvert, and Rick Shetter
National Center for Atmospheric Research, Boulder Colorado, USA

Received 7 March 2001; revised 10 September 2001; accepted 12 September 2001; published 8 March 2002.

[1] The relationship between photolysis frequencies derived from spectroscopic measurements of actinic fluxes and irradiances was determined during a coordinated measurement campaign (International Photolysis Frequency Measurement and Modeling Intercomparison campaign (IPMMI)). When differences in viewing geometries are taken into account, the measurements are in close agreement. An empirical relationship, which is useful for high sun (noon) conditions or for daily integrals, was found to convert irradiance data to photolysis frequencies. For low-sun conditions (large solar zenith angle), model calculations were shown to improve the accuracy. However, the input parameters to the model are site specific and the conversion depends on diffuse/direct ratios. During cloudy conditions, significant improvements in the conversion can be achieved by assuming the radiation field to comprise entirely diffuse isotropic radiation when the UVA transmission by cloud is less than 0.8. Changing cloud conditions remain the greatest limitation, but they tend to bias the results away from the clear-sky case in a systematic way. Furthermore, although the cloud effects on the photolysis rates of nitrogen dioxide ($J(NO_2)$) are rather large, they are much smaller for ozone photolysis ($J(O_3 \rightarrow O(^1D))$), which is of prime importance in tropospheric chemistry. The study shows the potential for deriving historical and geographical differences in actinic fluxes from the extensive records of ground-based measurements of spectral irradiance. *INDEX TERMS:* 0360 Atmospheric Composition and Structure: Transmission and scattering of radiation; 0365 Atmospheric Composition and Structure: Troposphere—composition and chemistry; 0368 Atmospheric Composition and Structure: Troposphere—constituent transport and chemistry; 0394 Atmospheric Composition and Structure: Instruments and techniques; *KEYWORDS:* photolysis, spectral irradiance, actinic flux, UV, ultraviolet radiation

1. Introduction

[2] Recently, instruments have been designed to measure spectrally resolved actinic fluxes directly [*Hofzumahaus et al.*, 1999; *Shetter and Müller*, 1999]. However, a much more extensive database of spectral irradiance measurements exists, with measurements extending back a decade or more at several sites [*Herman et al.*, 1999]. There have been several previous studies, which investigated how irradiances may be converted to actinic fluxes and photolysis frequencies. For example, empirical relationships have been discussed by *Madronich* [1987], *Nader and White* [1969], and *Van Weele et al.* [1995].

[3] The theoretical foundation for this transformation was outlined by *Madronich* [1987]. Early attempts to relate the two experimentally used broadband data rather than spectrally resolved measurements, and differences between the weighting functions was a source of uncertainty. More recently, spectral measurements have been compared with calculated actinic fluxes [*Kazadzis et al.*, 2000], but these were only for clear-sky conditions. That study demonstrated that under polluted conditions, significant overestimations of the derived actinic fluxes resulted when it was assumed that the diffuse beam component is isotropic. The purpose of the present study is to evaluate differences between spectrally resolved measurements based on cosine-weighted irradiances, compared with those measuring actinic fluxes directly, and thus to determine the extent to which such irradiance data can be used to derive actinic fluxes at the surface.

[4] In the summer of 1998, an International Photolysis Frequency Measurement and Modeling Intercomparison campaign (IPMMI) was held at Marshall Field (39.95°N, −105.20°E, altitude 1.65 km) near Boulder, Colorado, USA. The suite of instruments available was extensive, including chemical actinometers, broadband radiometers, and scanning spectroradiometers. Here we investigate relationships between results from the three scanning spectroradiometers, which were operated by groups from New Zealand's National Institute of Water and Atmospheric Research

[1]Now at Department of Pharmacokinetics, Grünenthal GmbH, Aachen, Germany.

0148-0227/02/2001JD000601

Table 1. Instrument Details

	NIWA Instrument	FZJ Instrument	NCAR Instrument
Reference	*McKenzie et al.* [1992]	*Hofzumahaus et al.* [1999]	*Shetter and Müller* [1999]
Entrance optic	Ptfe (Teflon) cosine diffuser	Quartz actinic diffuser	Quartz actinic diffuser
Quantity measured	Irradiance	Actinic flux	Actinic flux
Instrument	JYDH10	Bentham DTM300	CVI Digikrom 112
Focal length, mm	100	300	110
Grating, groove mm^{-1}	1200	2400	2400
Slit dimensions	0.25 mm × 6 mm	1.48 mm × 6 mm	4.2 mm × 0.6 mm
Wavelength range, mm	290–450	280–420	282–420
Resolution,[a] nm	1.3	1.1	1.0
Sampling step, nm	0.2	1.0	1.0, 2.0[b]
Detector, PMT[c]	EMI 9804 QA	EMI 9250 QB	EMI 9125A
Calibration Standard	1000 W FEL lamp	1000 W FEL lamp	1000 W QTH lamp
Reference laboratory	National Institute for Standards and Technology	Physikalisch Technische Bundesanstalt	National Institute for Standards and Technology
Scan duration, s	190	68	11
Repetition Rate, s	300	80	15
Measurement uncertainty, %	±6	±6	±6[d]

[a] Resolution is full width at half maximum.
[b] Value is 1.0 nm over the range 282–330 nm but increases to 2.0 for the interval 330–420 nm.
[c] PMT stands for photomultiplier detector.
[d] Value is 4.8% for UVA.

(NIWA), the Institut für Atmosphärische Chemie, Jülich (FZJ), Germany, and the National Center for Atmospheric Research (NCAR), USA.

2. Instrumentation

[5] All three scanning instruments are double monochromators configured for additive dispersion, which are coupled to the detector head via fiber-optic bundles. The instrument details for each of the above groups have been described elsewhere [*Shetter and Müller*, 1999; *Hofzumahaus et al.*, 1999; *McKenzie et al.*, 1992], but the important features are listed in Table 1. Modifications to the NIWA instrument include replacement of the original diffuser with an in-house-designed diffuser coupled to the instrument via a fiber optic bundle, resulting in a greatly improved cosine response. All three instruments scan the spectral region between 290 and 420 nm at a spectral resolution of approximately 1 nm. However, while the NIWA instrument uses a diffuser with a cosine response to measure the irradiance incident on a horizontal surface, the other two are equipped with diffusers designed to measure the actinic flux received from the full hemisphere. Since the ground albedo in the UV region is small, the flux measured by the instruments is a close approximation to the total actinic flux (from both hemispheres) when the detectors are close to Earth's surface. During the campaign the NIWA spectrometer was set up with its diffuser 2 m above the ground, while diffusers for the other two instruments were 5 m above the ground. All instruments had good views of the horizons. The irradiances provided from the NIWA instrument include small corrections factors, CF(λ, SZA), to account for departures from a true cosine response in the diffuser. These corrections take the form

$$\mathrm{CF} = \mathrm{CF}_{\mathrm{sky}}\, D + \mathrm{CF}_{\mathrm{sun}}(1 - D), \qquad (1)$$

where D is the diffuse fraction, defined as the ratio of diffuse/global irradiance; $\mathrm{CF}_{\mathrm{sky}}$ is the correction factor for assumed isotropically distributed sky radiation; and $\mathrm{CF}_{\mathrm{sun}}$ is the correction factor for direct sunlight.

[6] The diffuser on the NIWA instrument has an excellent cosine response, with $\mathrm{CF}_{\mathrm{sky}} = 1.012$ and $|\mathrm{CF}_{\mathrm{sun}} - 1| < 0.03$ for all SZA < 70°. At larger solar zenith angles (SZA), $\mathrm{CF}_{\mathrm{sun}}$ increases and exceeds 1.2 by SZA = 85°. The largest corrections applied for UVA during the campaign was CF = 1.03, which occurred at SZA ∼ 85°. The correction remains relatively small because under these conditions, most of the UV radiation is diffuse. Similarly in the UVB region, where there is a larger fraction of diffuse radiation, corrections are smaller than in the UVA region.

[7] Although all-sky camera records were available during the campaign period, there were no sky radiance measurements available. In the absence of such measurements, it was assumed that the diffuse sky irradiance was isotropic.

3. Discussion of Results

[8] Spectra were taken throughout the 4 days of the campaign in June 1998 (dates: 15, 16, 18, and 19 June). Typical spectra, taken near midday on 19 June, which was the only clear day, are shown in Figure 1. Not all groups collected sky spectra on 17 June, which was used as a calibration day. The three groups involved in this study all calibrated their instruments against quartz halogen lamps traceable to International Calibration standards. Because of differences in scanning speeds and hence the scan repetition rate between the three instruments, the data obtained were not precisely simultaneous, and this leads to some scatter in results during partly cloudy conditions when signals can change rapidly. Ozone retrievals were available from the spectra themselves using an algorithm described previously [*Stamnes et al.*, 1991]. Ancillary data were available, including measurements of ozone and aerosol optical depth from a Microtops instrument and ozone measurements from a Dobson spectrophotometer in nearby Boulder. Relevant parameters affecting UV radiative transfer are listed in Table 2.

[9] The results for the two instruments with actinic diffusers are in excellent agreement, given the differences in bandwidth and sampling intervals (note that the NCAR data are undersampled at λ > 330 nm; see Table 1). The photon flux rates are smaller for the NIWA instrument because irradiances ($E(\lambda)$) are generally smaller than actinic fluxes ($F(\lambda)$), which are independent of the angle of incidence.

[10] The curves in Figure 1b show spectral ratios of actinic fluxes to irradiances as measured by FZJ and NIWA (FZJ/NIWA)

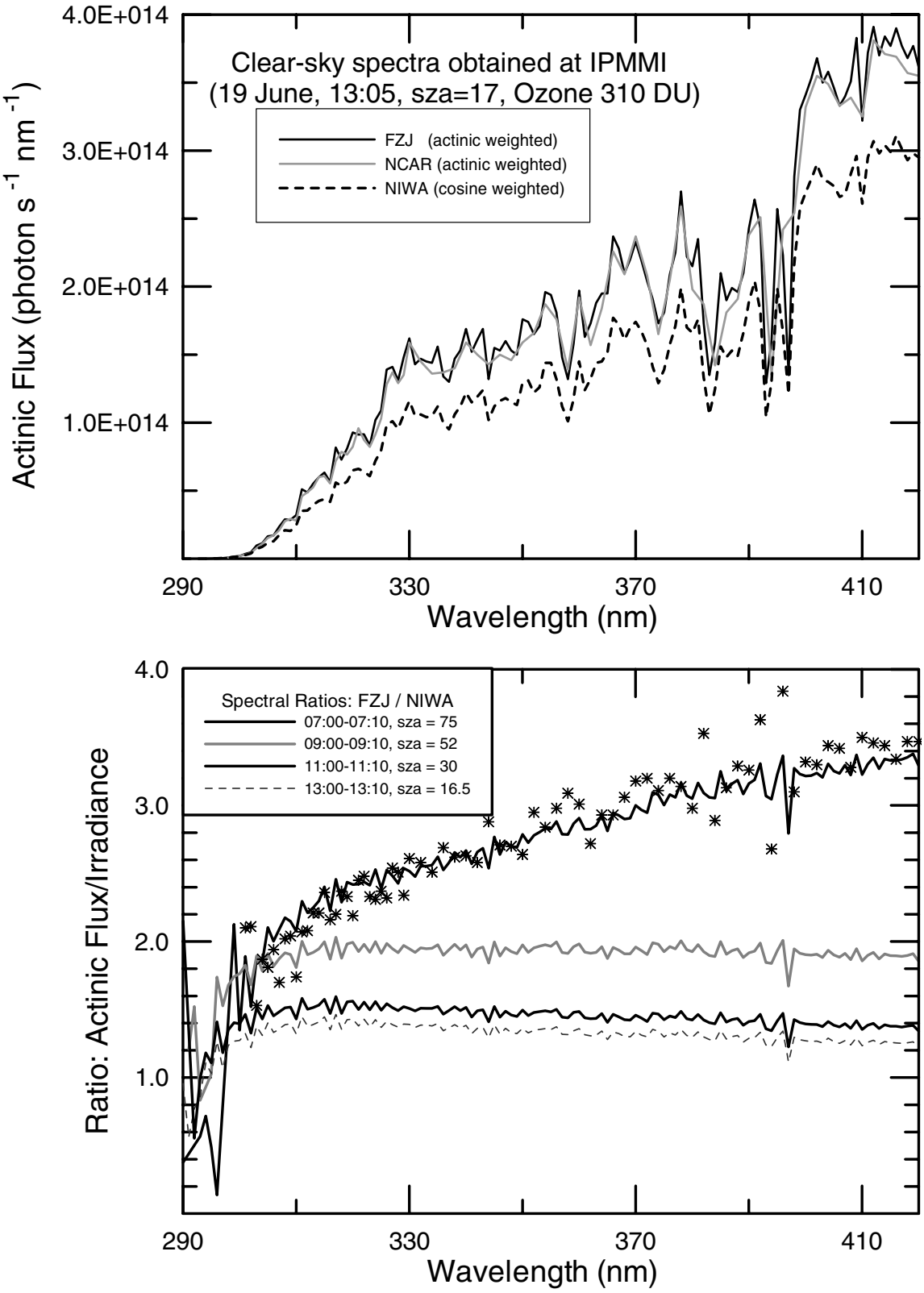

Figure 1. (top) Spectra measured by each instrument near solar noon (SZA = 17°, 13:05 MDT) on 19 June 1998. In this plot the *y* axis is plotted on a linear scale, and the sampling interval for the *x* axis is 1 nm, except at $\lambda > 300$ nm, where the National Center for Atmospheric Research (NCAR) sampling interval was 2 nm. (bottom) Spectral ratios of actinic flux divided by irradiances (Forschungzentrum Jülich/National Institute of Water and Atmosphere (FZJ/NIWA)) for several solar zenith angles (SZA). The asterisks on the upper curve show the ratios for NCAR/NIWA.

Table 2. Observing Conditions During the Measurement Campaign

Parameter	15 June	16 June	18 June	19 June
Day of year	166	167	169	170
Minimum SZA, degrees	16.6	16.6	16.5	16.5
Ozone from spectra, DU	350–360	340–345	370–320[a]	300–310
Ozone from Dobson, DU	350	330	345	309
1 μm aerosol optical depth	<0.05	<0.05	<0.05	<0.05
Surface pressure, hPa	830	820	826–830	829–824

[a] Over the course of the day, ozone decreased from 370 Dobson units (DU) to 320 DU.

respectively for several SZA on 19 June (clear skies). For SZA <30° the ratios at wavelengths greater than 300 nm remain approximately constant, with actinic fluxes being approximately 50% more than irradiances. As the SZA increases, the ratios increase, with actinic fluxes being nearly twice as large as irradiances when SZA = 52°. As the SZA continues to increase, the ratio of actinic flux to irradiance also increases. These results are qualitatively consistent with those calculated [*Madronich*, 1987]. Although the measured ratio at the largest SZA is somewhat higher than calculated, it should be noted that the calculation conditions are not identical. The residual higher-frequency structure in the curves is due to slight mismatches in band pass between the two instruments (see Table 1). This results in largest differences in regions where the spectrum is steepest (for instance, the deep solar Fraunhofer lines near 396 nm or the ozone cutoff below 300 nm). The asterisks plotted on the upper curve are ratios of NCAR/NIWA. These show larger departures because the mismatch between spectral resolutions is greater. These mismatches will also contribute to the decreases in the ratio at the shortest wavelengths where the spectrum is steepest. Because of differences in scan rate, ratios of this type taken on cloudy days are noisier.

[11] The photolysis frequency is defined as

$$J(\lambda) = \int F(\lambda)\sigma(\lambda)\eta(\lambda)d\lambda, \qquad (2)$$

where $F(\lambda)$ is the actinic flux (cm^{-2} s^{-1} nm^{-1}), $\sigma(\lambda)$ is the absorption cross section (cm^{-2}), and $\eta(\lambda)$ is the quantum yield for photolysis. To illustrate the differences between $J(O_3)$ and $J(NO_2)$, the spectral dependence of these photolysis frequencies are shown for Figure 2 for the midday spectrum on 19 June. In the case of O_3 photolysis to produce $O(^1D)$ the peak is in the UVB region, whereas in the case of NO_2 photolysis the peak is in the UVA region.

[12] Integrals over wavelength were used to represent the actinic flux for ozone photolysis and NO_2 photolysis (Table 3), and results were submitted as 10-min means to the campaign referee. There was no opportunity to compare results before submitting the data, making this a blind intercomparison. For spectral data a common wavelength grid spacing of 1.0 nm was used for all instruments in the submitted data. In the case of the NIWA instrument, which measured irradiances, we designate the photolysis frequencies derived from these irradiances as "pseudo photolysis frequencies" (J_{pseudo}) to distinguish them from true photolysis frequencies (J) based on actinic flux measurements. Conversions to true photolysis frequencies will be discussed further in section 5.

[13] The diurnal variations of $J(O_3)$ and $J(NO_2)$ for 2 days during the campaign are shown in Figure 3. The first day (15 June) was clear until midmorning and then became partly cloudy. By mid-afternoon it was fully overcast. In contrast, the last day of the campaign (19 June) was cloud free, apart from a few cumulus clouds that built up in the late afternoon. There is good agreement throughout the day for the two instruments that measured actinic fluxes, particularly on 19 June. On 16 June, The FZJ instrument gave values 5–10% higher than the NCAR instrument. However, these differences are within the combined range

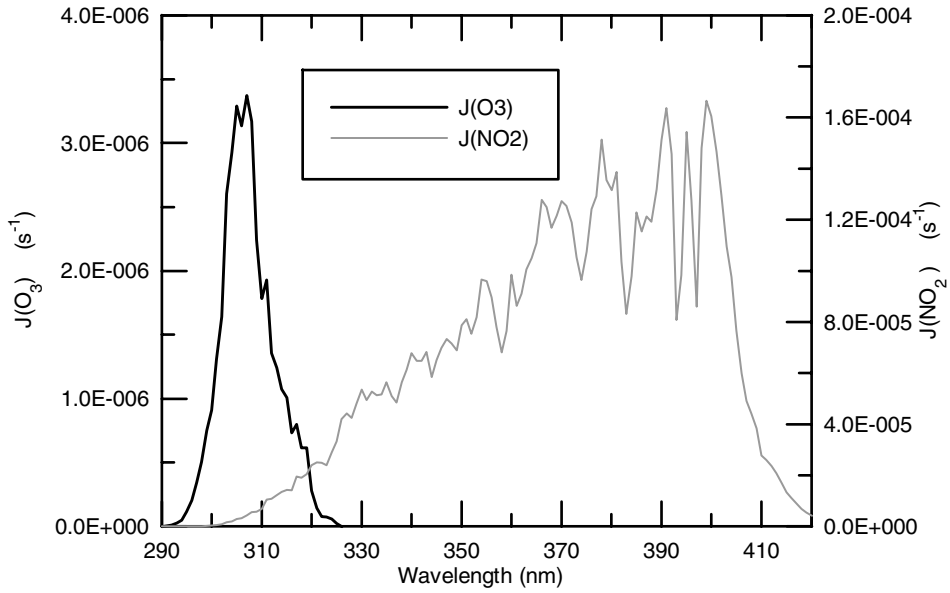

Figure 2. Spectral photolysis frequency, $J'(O_3) = dJ(O_3)/d\lambda$ and $J'(NO_2) = dJ(NO_2)/d\lambda$, derived from the spectrum measured by the NIWA instrument at solar noon on 19 June 1998. To generate this plot, the NIWA spectrum has been converted to actinic flux as discussed in section 5.

Table 3. Details of Photolysis Frequencies Considered

Photolysis Frequency, J	Absorption Cross Section σ(λ) Reference	Quantum Yield η(λ) Reference	Temperature
$J(O_3)$: $O_3 + h\nu \rightarrow O(^1D) + O_2$	*Molina and Molina* [1986]	*DeMore et al.* [1997]	T-actinometer
$J(NO_2)$: $NO_2 + h\nu \rightarrow NO + O$	*Harder et al.* [1997]	*DeMore et al.* [1997]	298 K

of experimental uncertainties (see Table 1). The NIWA instrument showed the same general patterns, but, as expected, the irradiances were consistently lower than the actinic fluxes. At noon the actinic fluxes were approximately 35% larger than the pseudo-fluxes based on irradiances.

[14] The NO_2 photolysis frequencies at noon were more than 20 times larger than the O_3 photolysis frequencies, and the differences became more pronounced at larger solar zenith angle (SZA) where Rayleigh and ozone extinctions reduced the O_3 photolysis frequency more rapidly than the NO_2 photolysis frequency. Cloud effects are significantly larger in the case of NO_2 photolysis.

[15] In Figure 4 the J values based on actinic fluxes have been plotted as a function of the pseudo J values based on irradiances. In both cases the clear sky data are tightly grouped about polynomial regression lines, which can be used to empirically relate irradiances to actinic fluxes. The regression lines are

$$J = a + bJ_{\text{pseudo}} + cJ^2_{\text{pseudo}} + dJ^3_{\text{pseudo}} \tag{3}$$

where J_{pseudo} is the value derived from the irradiances.

[16] The best fit values for the parameters for these observing conditions are given in Table 4. A quadratic function is sufficient to accurately model the dependence in the case of $J(O_3)$. However, in the case of $J(NO_2)$ the relationship is more complex, and a cubic polynomial is preferred (see Figure 4). The functions derived are very similar for the two instruments, and in the case of $J(O_3)$ are difficult to distinguish on the plot.

[17] In the case of $J(NO_2)$, there is a relatively large spread about this line with a tendency for values below the line during

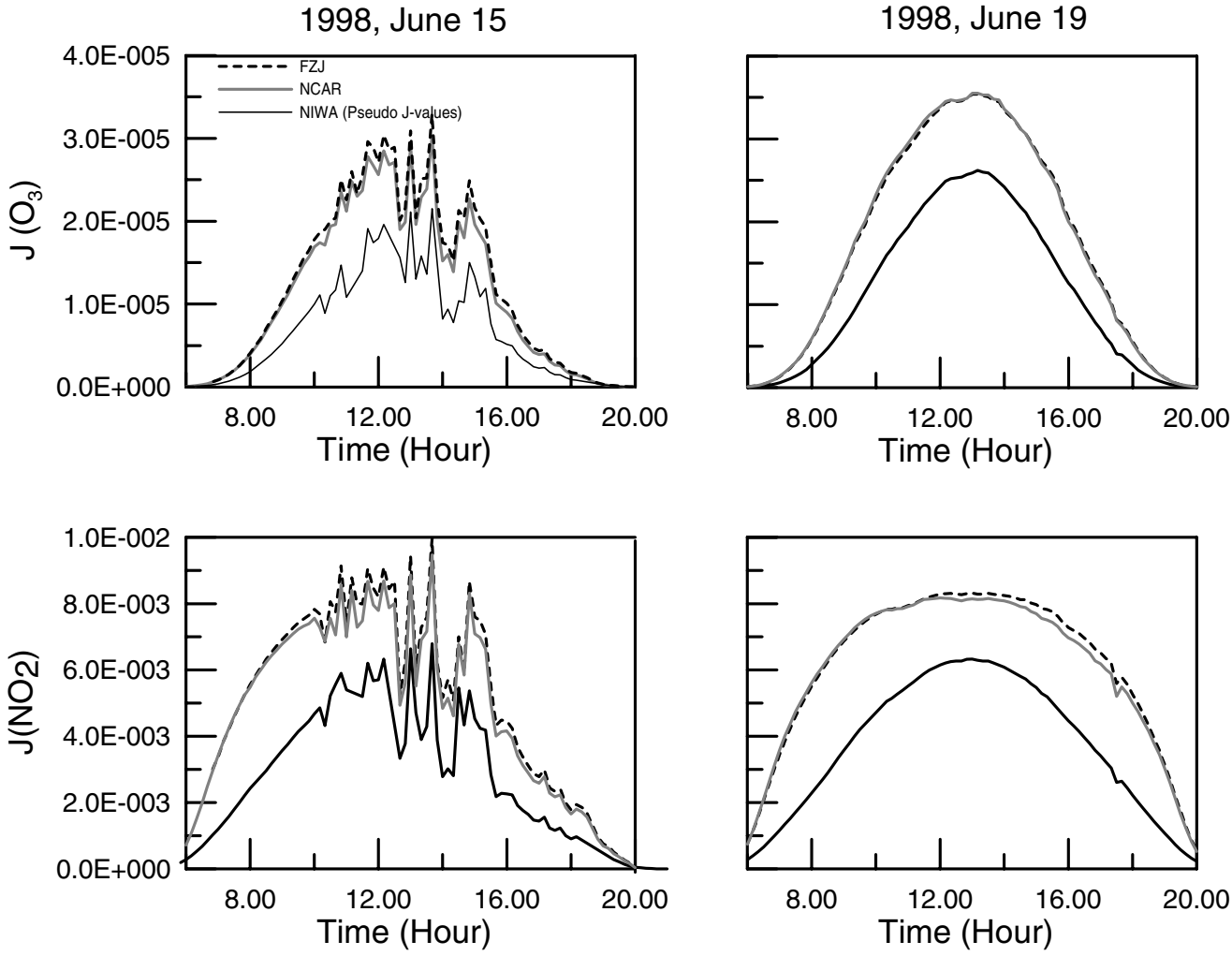

Figure 3. Diurnal variation of photolysis rates for 2 days. The NIWA instrument values are pseudo-photolysis rates, as discussed in the text. The top panels show $J(O_3)$, and the bottom panels show $J(NO_2)$. In each case the y axis labeling on the left panel applies also to the right panel.

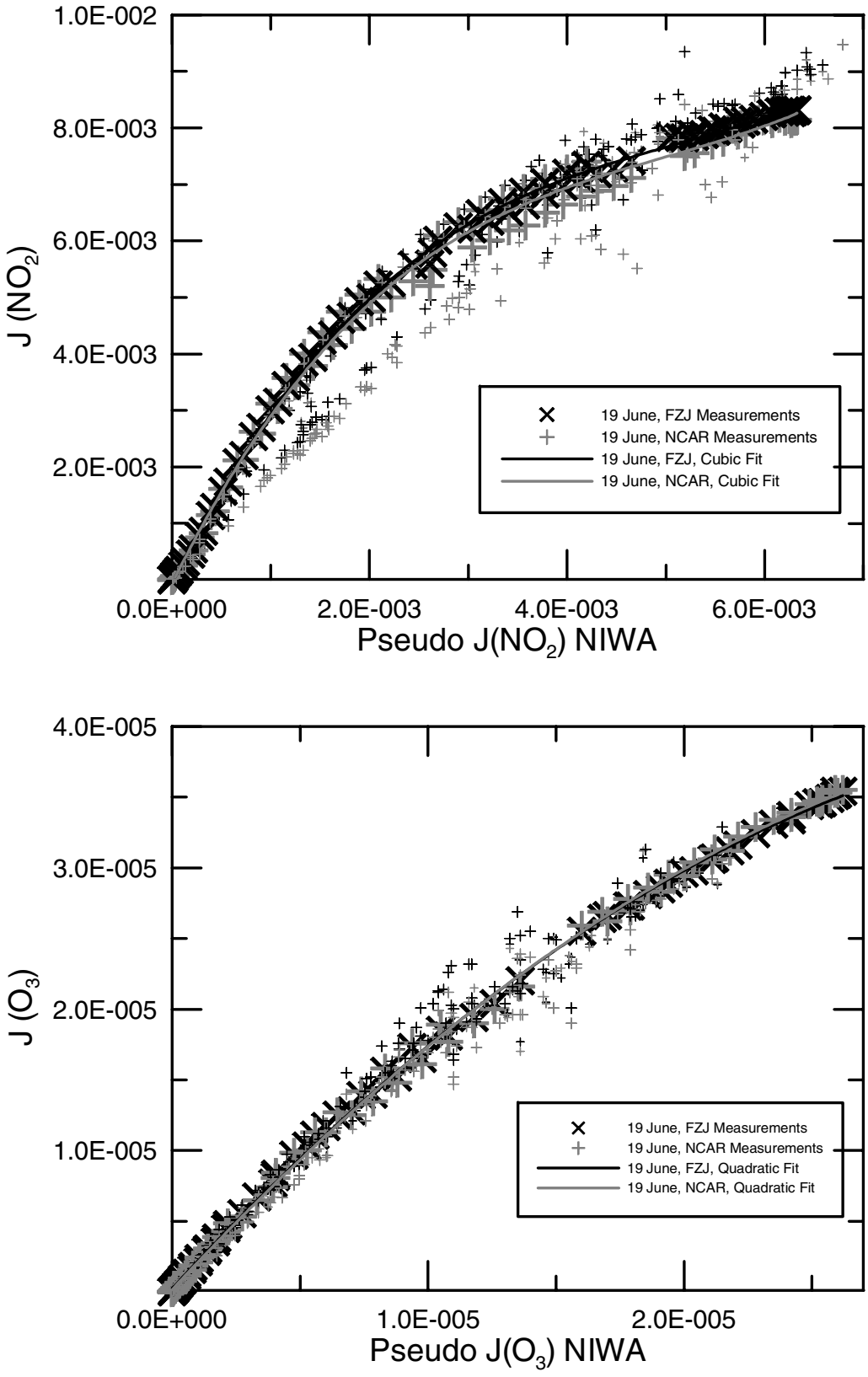

Figure 4. Scatterplot of *J* values based on actinic fluxes plotted as a function of the pseudo *J* values based on irradiances. Crosses and the fitted lines apply to data from the clear day (19 June). Plus symbols are for the other days.

Table 4. Parameters Describing the Best Fit Polynomial Regression Between Photolysis Frequencies and Pseudo-Photolysis Frequencies[a]

	a	*b*	*c*	*d*
$J(NO_2)$	0	3.56	−596.4	38,652
	0	3.54	−608.4	40,701
$J(O_3 \rightarrow O(^1D))$	0	1.95	−23,766	0
	0	1.95	−23,358	0

[a] Values in the first rows are based on FZJ data; the second-row values are based on NCAR data.

cloudy conditions. Partly cloudy conditions at noon, however, lead to larger increases in the actinic fluxes. By contrast, in the case of $J(O_3)$ the points are tightly grouped about the regression line for all cloud conditions. There is a tendency for values to lie above the regression line during cloudy conditions, and there is no evidence of cloud-enhanced values near noon.

[18] The above treatment gives a good indication of the agreement that can be achieved for daily integrated *J* values. However, under twilight conditions, where *J* values become small, the differences may still be appreciable. To investigate these in more detail, we consider ratios between *J* values and the pseudo *J* values.

[19] Figure 5 shows ratios of *J* values divided by the NIWA pseudo *J* values measured as a function of time over 2 days. Near noon the ratios are close to 1.35 as noted previously and are similar for both $J(NO_2)$ and $J(O_3)$. On the clear day, similarity continues for SZA < 60°, probably because the radiation field is dominated by radiation from near the solar direction. At larger SZA the ratios tend to increase, especially in the case of $J(NO_2)$ where the ratio reaches a maximum of approximately 3 for clear sky conditions (for SZA 78° to 80°). At larger SZA, the ratios tend to decrease and are smaller for $J(O_3)$ because at these larger SZA the radiation field tends to become more diffuse and isotropic at the shorter wavelengths [*Blumthaler et al.*, 1996]. There is a suggestion that the effects of clouds on these corrections for $J(O_3)$ are anticorrelated with those for $J(NO_2)$. However, differences in sampling time may also be a contributing factor.

[20] Up to this point, we have directly compared photolysis frequency measurements, with "pseudo-photolysis frequency" measurements from a cosine-weighted instrument, as submitted to the IPMMI campaign referees. There are strong correlations between the two, showing that (under these observing conditions) photolysis frequencies can be derived from the irradiance measurements. However, while there is little scatter when the SZA is small, the relationship is nonlinear, and errors escalate at larger SZA, and under cloudy conditions (Figures 4 and 5). These errors may be due to differences in the distribution of diffuse skylight, as discussed further in section 4.

4. Diffuse Fraction

[21] The irradiance measured by the NIWA spectrometer includes contributions from both the direct solar beam and from diffuse scattered light. The conversion from irradiance to actinic flux depends critically on the diffuse fraction, which varies as a function of wavelength and of SZA: the proportion of diffuse light increasing at shorter wavelengths and at larger SZA [*Zeng et al.*, 1994]. The diffuse fraction can be obtained by direct measurement or, if the necessary input parameters are known, from radiative transfer calculations.

[22] The diffuse fraction calculated with the pseudo-spherical discrete-ordinate version of "tropospheric ultraviolet" radiative transfer model [e.g., *Zeng et al.*, 1994] is shown for several SZA in Figure 6 (model input parameters are altitude 1.6 km and aerosol in the lowermost kilometer $\alpha = 1.7$, $\beta = 0.01$; with dustlike particles of single scattering albedo equal to 0.5, asymmetry parameter equal to 0.45, and ground albedo equal to 0.05, all independent of wavelength).

[23] Although diffuse fractions were not routinely obtained during this campaign, there were occasional measurements and examples are shown in Figure 6. For the observation at SZA = 63° the measured diffuse fraction shows reasonable agreement with the calculated ratios, except at wavelengths shorter than around 310 nm when the measured ratios decrease. The ratios measured near the middle of the day (SZA = 20°) show a similar wavelength dependence to the model, but the ratios are larger by about 0.07. We experimented with the model input parameters to try to reproduce the observed diffuse fractions at these two SZAs but found that to obtain agreement between the two, it was necessary to use unrealistic choices of the model parameters. Furthermore, these choices of input parameters led to inconsistencies between model and measurement at larger SZAs.

[24] The reason for the discrepancy is that there were procedural errors in the experimental determination of the diffuse ratios. At the time of measurement we had assumed that radiation incident near the edges of the diffuser could be ignored. Further experiments after the campaign showed that this assumption was incorrect. The diameter of the shading disk used during the IPMMI campaign disk was slightly smaller than that of the diffuser so that the shaded "diffuse" measurement included a contribution from direct sunlight incident on the edge of the diffuser. This resulted in an overestimation of the diffuse fraction. At the larger SZA the shadow was more elliptical, resulting in better obscuration of the solar disc, and a smaller error in the diffuse ratio.

[25] The diffuse fractions shown in Figure 6 apply only during clear skies. Under partly cloudy conditions the contribution of diffuse radiation is complex; however, provided the solar disk is visible, it may be appropriate to continue to use the ratios shown in Figure 6. When the sun is obscured by clouds, the radiation field is totally diffuse ($D = 1$). The threshold for switching to this value was set by comparing the measured UVA irradiance with the calculated UVA irradiance. The frequency distribution of this UVA transmission ($UVA_{Tr} = UVA_{measured}/UVA_{calculated}$) measured during the IPMMI campaign is shown in Figure 7. The distribution is bimodal, with the lower peak corresponding to sun-obscured conditions and the higher peak corresponding to sun-unobscured conditions. The nodal point between these two peaks occurs near $UVA_{Tr} = 0.8$. Similar bimodal distributions have also been noted at other sites [*McKenzie et al.*, 1998]. We therefore used as a discriminator for sun-obscured measurements: if $UVA_{Tr} < 0.8$, then $D = 1$.

5. Converting Irradiances to Actinic Fluxes

[26] In an attempt to see whether improvements can be made, we used a model to derive the geometric conversion factor to convert from irradiances to actinic fluxes as described below.

[27] To convert irradiances (E) to actinic fluxes (F), corrections need to be applied separately to the direct beam component and the diffuse component. Given the diffuse fraction, the actinic flux, in principle, can be derived from the irradiance using

$$\begin{aligned} F &= E_{\text{direct}}/\cos(\text{SZA}) + E_{\text{diffuse}}/r \\ &= E\{(1-D)/\cos(\text{SZA}) + D/r\}, \end{aligned} \tag{4}$$

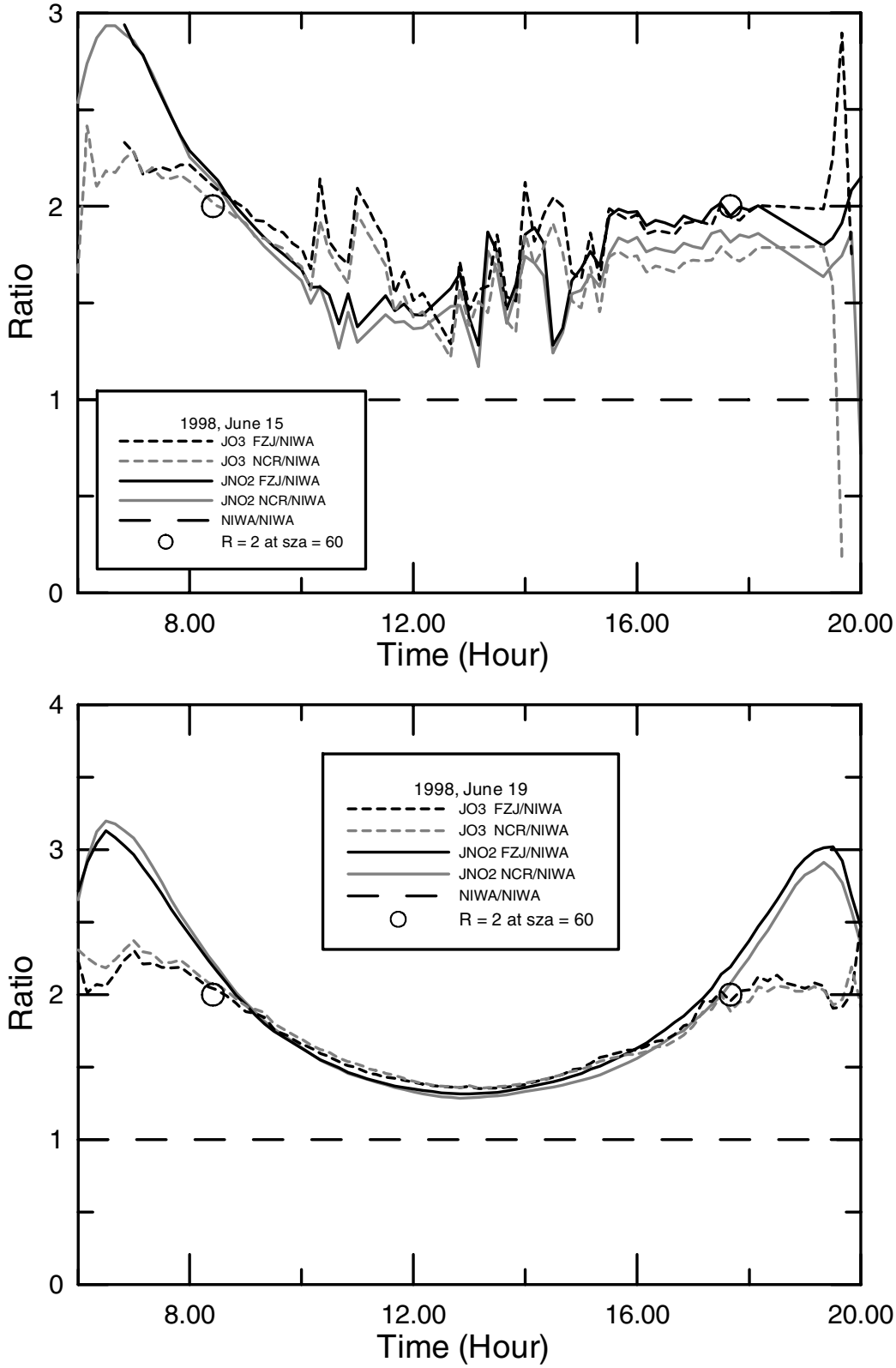

Figure 5. Ratios of J values divided by the pseudo J values measured as a function of time over 2 days. The SZA = 60° observations occurred at approximately 08:23 and 17:40 MDT on both days.

where r is the ratio of diffuse irradiance to diffuse actinic flux. As well as its dependence on wavelength and SZA, r also depends on atmospheric parameters such as cloud and aerosol extinction. Its value has been evaluated under a range of conditions, as discussed previously [*Madronich*, 1987; *Ruggaber et al.*, 1993; *Van Weele et al.*, 1995; *Hofzumahaus et al.*, 1999]. For isotropically scattered radiation, $r = 0.5$, whereas for vertical beam radiation, $r = 1.0$. In many cases the diffuse light is more intense at larger zenith angles

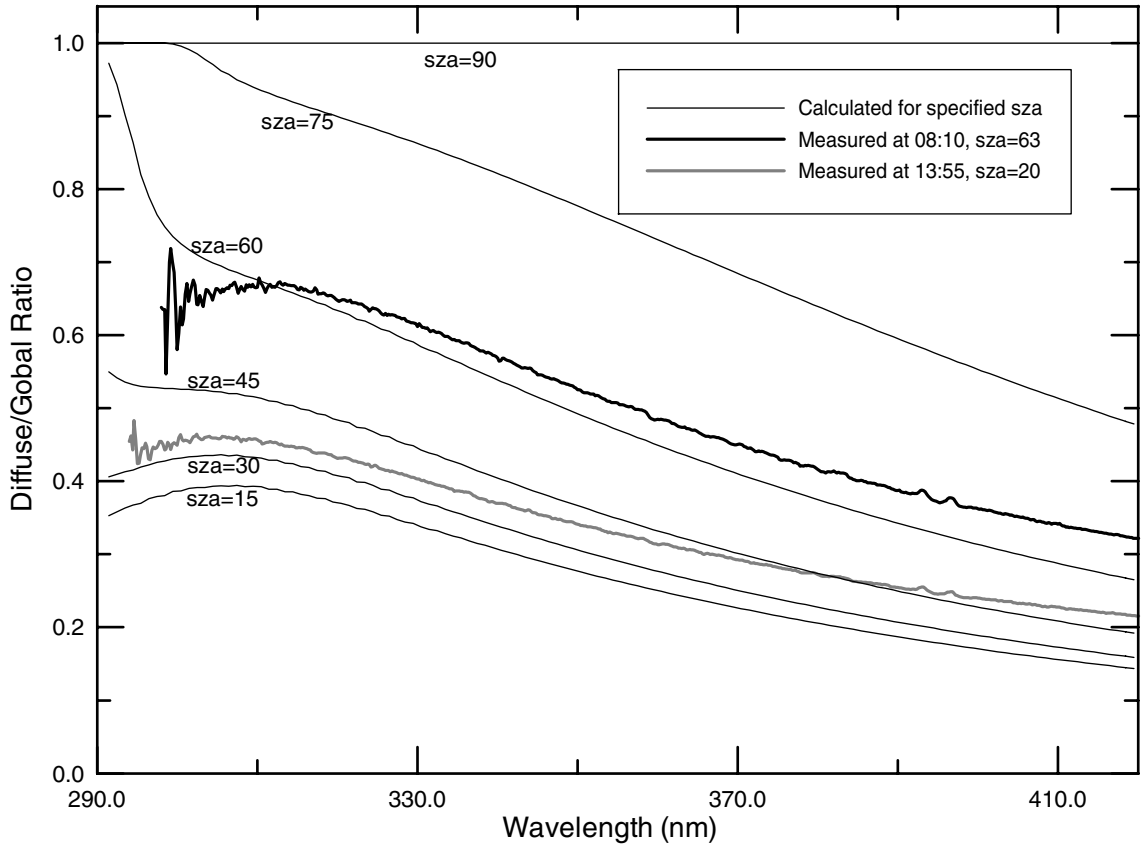

Figure 6. Diffuse/Global spectral ratios from measurements during clear-sky conditions on 19 June. Data are truncated at the short-wavelength detection threshold limit. Values calculated with a simple single-layer model are shown for comparison.

(horizon brightening), and in this case, $r < 0.5$. This horizon brightening becomes more important at larger SZA and at longer wavelengths, especially if aerosol scattering is significant [*Blumthaler et al.*, 1996; *Ruggaber et al.*, 1993]. For the unpolluted observing conditions during the IPMMI campaign, with aerosol optical depths (T_{aer}) close to zero and an altitude of 1.6 km, the diffuse radiation at $\lambda = 300$ nm is nearly isotropic giving $r = 0.5$, whereas at $\lambda = 400$ nm the radiation from the horizon is greater, giving $r \approx 0.4$ [*Ruggaber et al.*, 1993]. To approximate this dependence, we used

$$r = 0.5 - (\lambda - 300)/1000 \quad (5)$$

This function would need further modification for other observing altitudes or aerosol optical depths. Horizon brightening increases with optical depth, and this causes a reduction in the value of r. It has been shown [cf. *Ruggaber et al.*, 1993, Figures 7 and 9)] that even for hazy atmospheres the reductions in r are relatively small. It may therefore be appropriate to generalize the expression to

$$r = (0.5 - (\lambda - 300)/1000)(1 - n\ T_{aer}), \quad (6)$$

where n would need to be determined empirically. Under conditions of high aerosol concentrations, quantification of the diffuse component and departures from isotropy of the diffuse component become important [*Kazadzis et al.*, 2000]. The calculated values of r also depend on SZA [*Ruggaber et al.*, 1993]. However, for the observing conditions during the IPMMI campaign, this SZA-dependence is relatively small and has not been included here. There will be limitations to the applicability of this procedure. First, localized changes in sky intensity due to the presence of clouds are not considered. Second, errors could arise if the intensity changes rapidly during the spectral scan, especially in the case of $J(O_3)$ which is dominated by UVB rather than UVA radiation used to determine the above transmissions (see Figure 2).

[28] The plots above (for example, see Figure 5) show a pattern broadly consistent with this simple theory. At noon, when most of the light is direct, approximately half the radiation is scattered light. To convert this to actinic flux, the scattered light needs to be scaled up by a factor of 2 ($1/r$, where $r = 0.5$), assuming isotropic radiation fields. At larger SZA, the actinic flux becomes proportionately larger because the fraction of diffuse light increases and the correction for the direct component also increases. For $J(O_3)$, where the UVB radiation dominates, the actinic flux at large SZA is dominated by the diffuse component, so the correction tends toward a value of 2 ($1/r = 0.5$), which is smaller than for $J(NO_2)$ which is dominated by UVA radiation for which the direct beam component is more important.

[29] The processing of UV data from the NIWA instrument was modified to implement an option to apply the above algorithm, and the data were reprocessed to derive actinic fluxes from the measured irradiances. Figure 8 shows the spectrum of actinic flux thus derived from the irradiance data compared with the direct measurements of actinic flux. There are differences in details of the spectra, which are due to differences in the bandwidth of the three systems (see Table 1). However, excluding these differences, there is good agreement between the two methods, showing that for these observing conditions the maximum differences are within the combined measurement uncertainties (Table 1).

[30] The diurnal variations of $J(NO_2)$ and $J(O_3)$ as shown previously in Figure 3 are replotted in Figure 9, this time including the photolysis frequencies derived using the above procedure. As can be seen from (4) and (5), the conversion from irradiance to

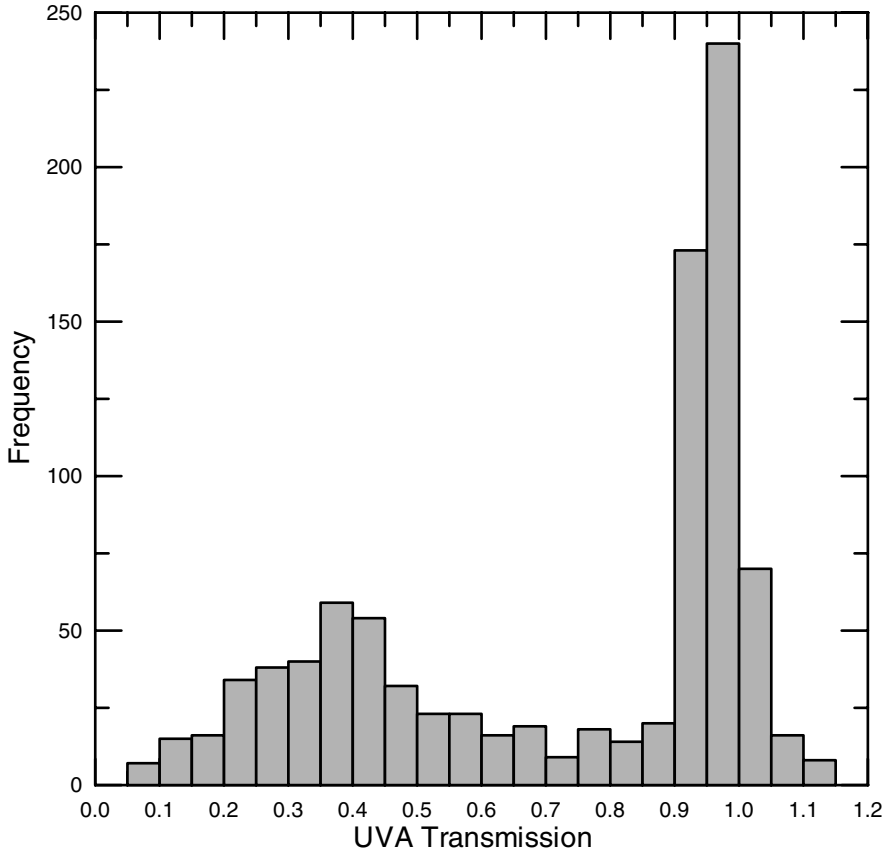

Figure 7. Histogram of UVA transmission though clouds and aerosols derived by comparing measured and calculated clear-sky UVA irradiance (315–400 nm) for all scans at SZA < 75° during the IPMMI campaign.

actinic flux is rather sensitive to D and r. The effects of errors in D are relatively small. A 20% increase in D leads to an increases in $J(NO_2)$ and $J(O_3)$ of ~5–10% for observations at low SZA (i.e., near midday). For observations around SZA = 60° the effect is near zero, and for larger SZA, increases in Dlead to decreases in photolysis rates. The effect of differences in r is also significant. If it is assumed that $r = 0.5$ at all wavelengths, rather than reducing from 0.5 to 0.4 over the interval 300– 400 nm, there are only minor differences in $J(O_3)$, but $J(NO_2)$ is reduced by about 10%, so that it more closely approximates the results for FJZ data around noon. During cloudy skies the agreement with direct measurements is poorer. However, it has been greatly improved by our assumption that the radiation field is diffuse ($D = 1$) when the UVA transmission is less than 0.8. Without this assumption the derived actinic fluxes during cloudy conditions would be reduced by >40%. For example, at 14:00 on 15 June the derived $J(NO_2)$ would be approximately 40% lower. Reductions in $J(O_3)$ are not quite as dramatic but still exceed 25%.

6. Instrument Intercalibration

[31] For SZA = 60° the correction for the direct beam cosine-weighted irradiance is expected to most closely match that for isotropic diffuse radiation. Consequently, observations at SZA = 60° may be used to provide the most direct intercalibration between the measurements from cosine-weighted readings and the actinic-weighted measurements. The actinic fluxes should be approximately twice the irradiances, as is observed in data from 19 June, where SZA = 60° occurs at 08:25 and at 17:40 Mountain Daylight Time (MDT) (all time are given in MDT; MDT = MST + 1 = UTC − 6) (see Figure 5). As the SZA diverges from 60°, errors in partitioning the diffuse fraction become more important. The ratios of J values are plotted as a function of SZA in Figure 10, using the FZJ data as the reference. The FZJ instrument was chosen as the reference in preference to the NCAR instrument because its scan rate is more similar to the NIWA instrument and because of its greater sensitivity (see Table 1). However, similar agreement results if the NCAR instrument is used as the reference. In the case of $J(NO_2)$ the derived results agree slightly better with the NCAR results, whereas in the case of $J(O_3)$ the derived values agree slightly better with the FZJ results.

[32] For both $J(NO_2)$ and $J(O_3)$ the ratio is close to unity over a range of SZA, including SZA = 60° during clear-sky conditions (e.g., 19 June), showing the calibration against the irradiance standards to be in good agreement. However, on cloudy days there are significant departures from unity, with a tendency toward larger ratios at small SZA (near noon). In the case of $J(O_3)$, there is a symmetric scatter about the clear-sky case, with most values being within 10–15% of unity, up to SZA ~85°. In the case of $J(NO_2)$, there is a tendency toward larger ratios on cloudy days. Since these systematic differences also occur at SZA = 60°, it follows that they arise from departures from isotropy of the diffuse radiation rather than from partitioning the diffuse fraction. Larger values in the ratio are consistent with skies being darker near the horizons, where the sensitivity to cosine-weighted irradiances is relatively small. The systematically larger cloud-induced errors for $J(NO_2)$ than for $J(O_3)$ are consistent with the greater sensitivity of D at UVA wavelengths compared with values near 0.5 more typical of the UVB wavelengths (see Figure 6).

[33] Smaller ratios for $J(NO_2)$ were seen on the clear day (19 June) at SZA = 80° to 85° both in the morning and afternoon data (see Figures 10 and 11). Similarly low values were seen at the same time in the clear morning of 16 June, and in each case, low values

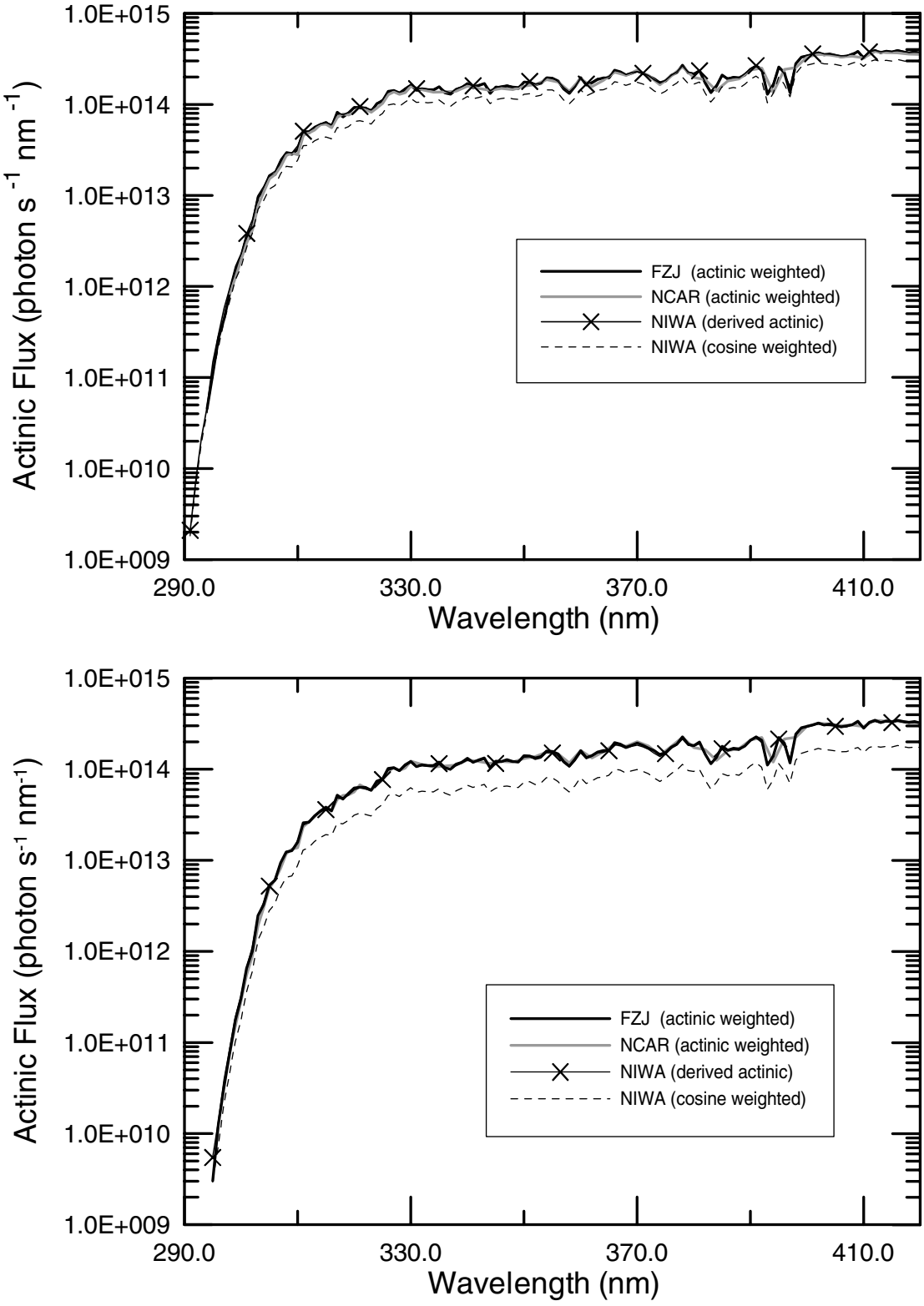

Figure 8. Spectral irradiance data from the NIWA instrument plotted on a logarithmic *y*axis scale and the same spectra converted to actinic flux and compared with the direct measurements from the instruments that measured actinic flux directly for measurements at two SZA on 19 June 1998: (top) SZA = 17° at 13:05 and (bottom) SZA = 52° at 09:05. Details of three of the curves in the top panel can be seen more clearly in Figure 1, which is plotted on a linear scale.

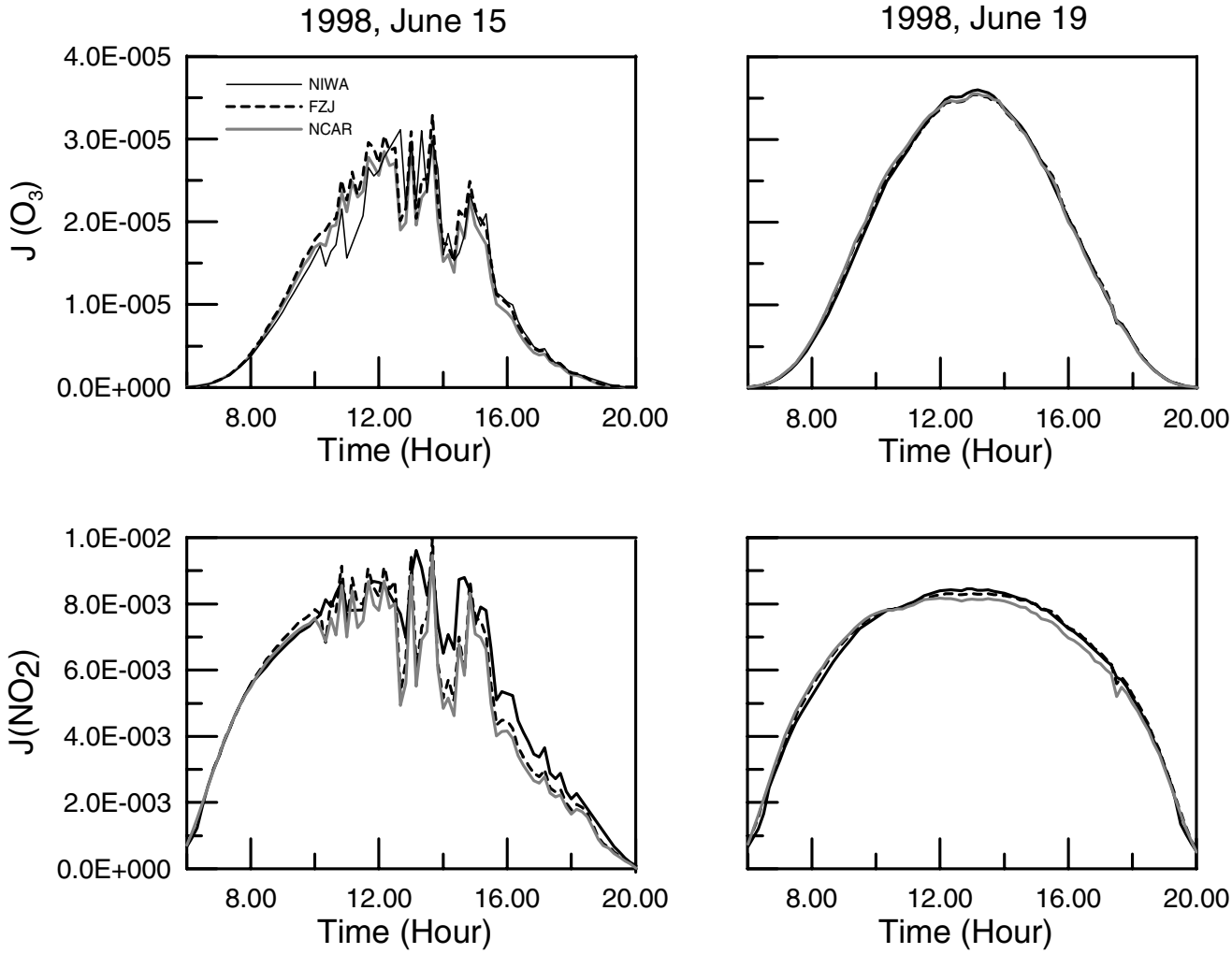

Figure 9. Diurnal variation of derived photolysis rates for 2 days. The top panels show $J(O_3)$, and the lower panels show $J(NO_2)$. In each case the y axis labeling on the left panel applies also to the right panel.

also occurred when using the NCAR instrument as the reference, indicating that the anomaly was due to low values derived from the NIWA instrument. The error can be traced back to escalating errors in the cosine response of the instrument at these large SZA. Between SZA 80° and 85° the relative cosine response reduces from 0.93 to 0.77. Although a correction is applied, as discussed in section 2, it assumes that the scattered light is isotropic, which is clearly not the case under these twilight conditions. The errors are exacerbated by obstructions that preferentially block the direct sun from the NIWA instrument, which was mounted 3 m below the others. In the mornings a shadow was cast by meteorological equipment on the ground at an azimuth of 60°, while in the afternoon, the hills in the west tend to block more of the radiation field than to the other instruments.

[34] At SZA larger than ~86° the anomaly is no longer present because the direct component is by then small enough to have little influence on any of the instruments. At these large SZA the photolysis frequencies are small compared with their midday values (see Figure 9), so the discrepancies of ~20% would lead to only small errors in daily doses.

[35] The anomaly does not occur in the $J(O_3)$ data for which the direct beam component at this SZA is small. Similarly, errors due to anisotropy arising from clouds are less severe in the case of ozone photolysis, which is more dominated by UVB radiation so that the contrast between cloud and sky is less pronounced. This may also be a contributing factor to the $J(O_3)$ ratios remaining close to unity up to SZA ~90°, a somewhat larger range than in the case of $J(NO_2)$.

[36] Figure 11 also shows that the NIWA-derived values tend to increase by ~5% over the day, using either FZJ or NCAR instrument as the reference. This behavior may be the result of a calibration drift or leveling errors in the NIWA instrument. Alternatively, it may be due to systematic changes in the radiation field caused by changes in aerosols throughout the day or by changes caused by the proximity of mountain ranges to the west. When the data are displayed as a scatterplot (Figure 12), this results in some separation between the prenoon and postnoon data. However, the differences are small compared with the differences due to sky anisotropy caused by clouds.

7. Conclusions

[37] For clear skies at SZA = 60° the observed ratio J/J_{pseudo} = 2, as predicted by simple theory giving confidence in the radiometric calibration accuracy of the three spectral instruments that measured the photolysis frequencies of NO_2 and O_3 during the IPMMI campaign. Under clear sky conditions, irradiance measurements during daylight hours (up to SZA ~80°) made at this site during IPMMI can be converted to actinic fluxes to derive photolysis frequencies for $J(O_3)$ and $J(NO_2)$ with an additional

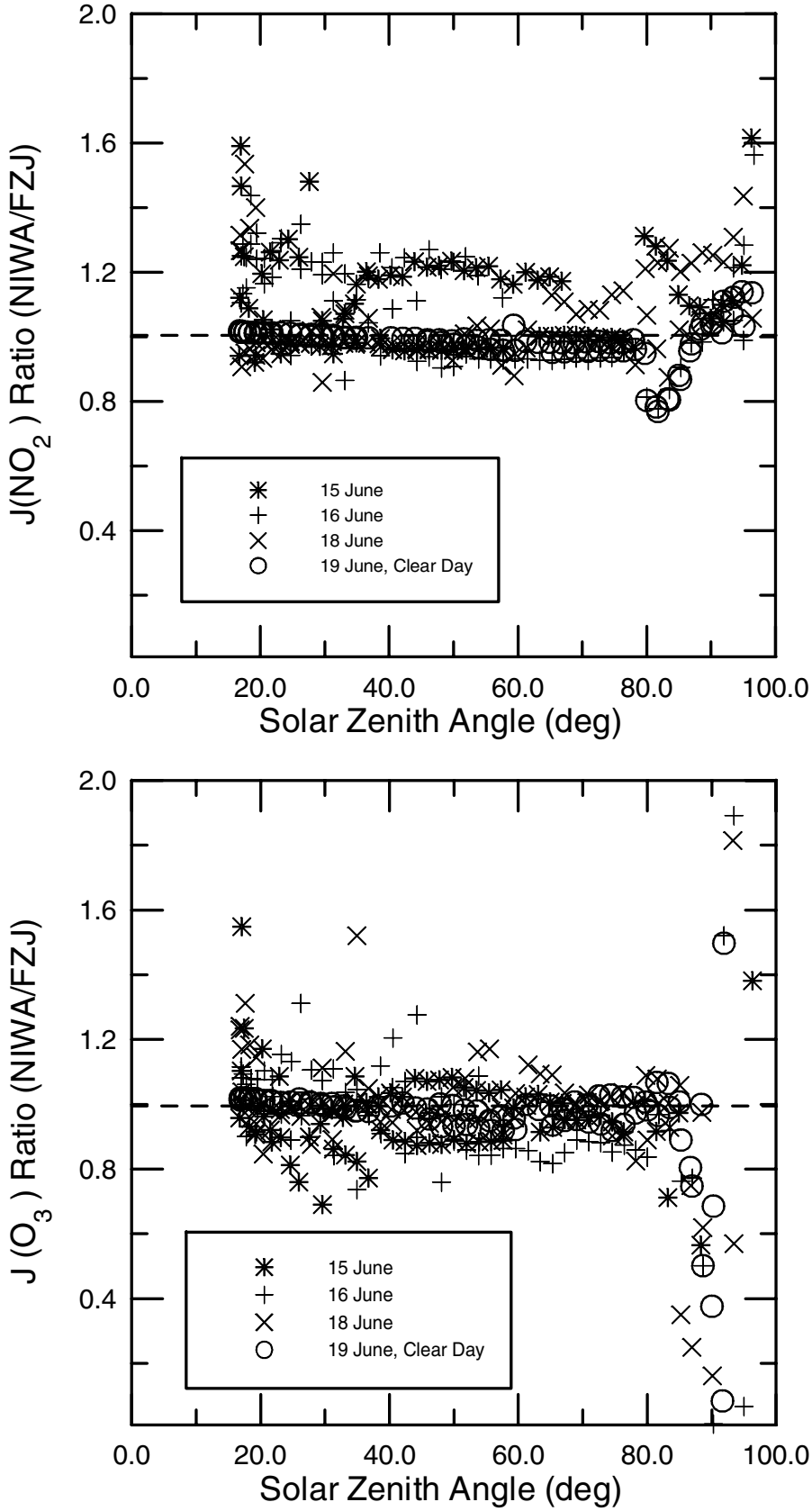

Figure 10. Ratios of J values with respect to a reference instrument (FZJ) as a function of SZA: (top) $J(NO_2)$ and (bottom) $J(O_3)$.

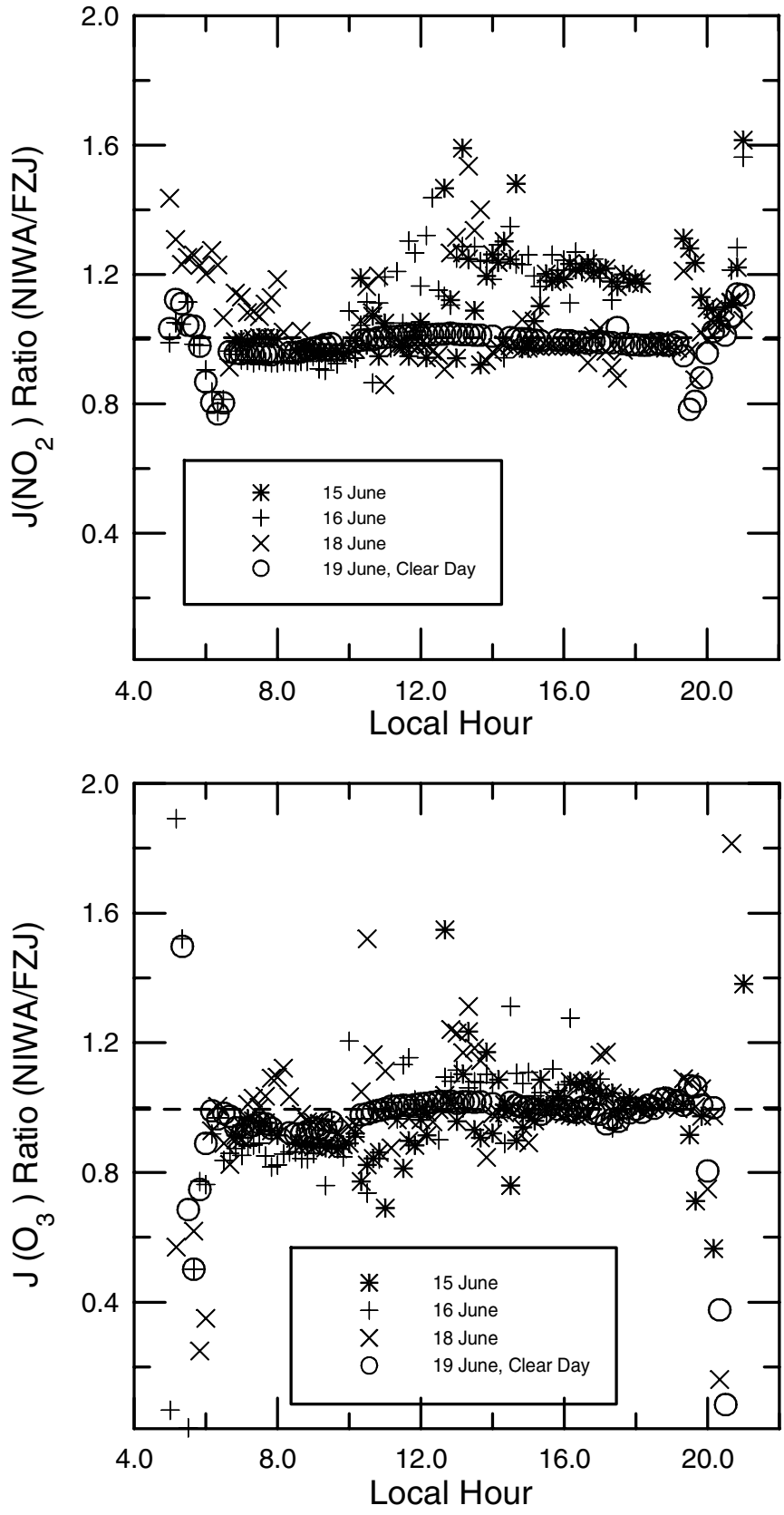

Figure 11. Ratios of J values with respect to a reference instrument (FZJ) as a function of time: (top) $J(NO_2)$ and (bottom) $J(O_3)$. This figure should be contrasted with Figure 5.

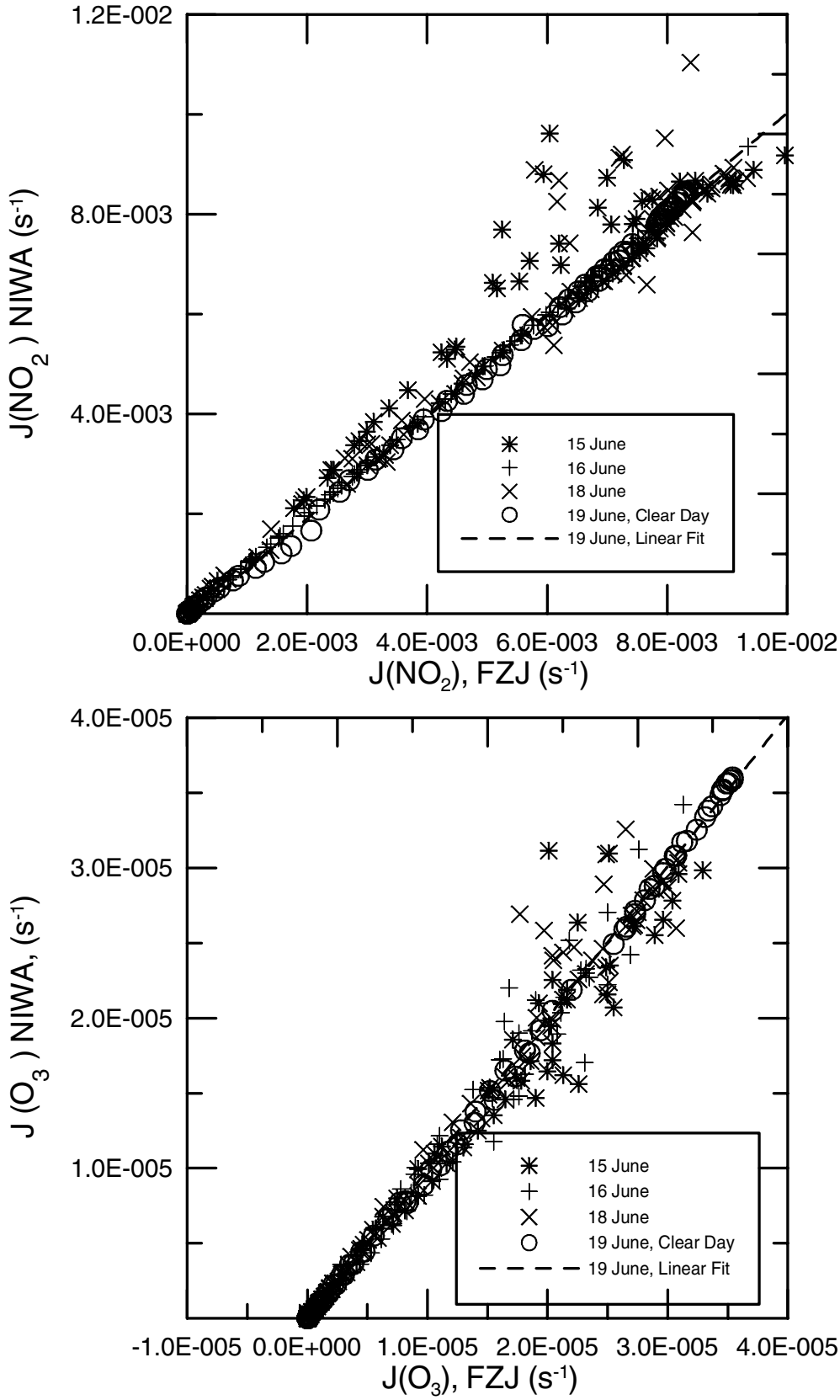

Figure 12. Scatterplots of model-corrected pseudo J values compared with measured J values: (top) $J(NO_2)$ and (bottom) $J(O_3)$. This figure should be contrasted with Figure 4.

uncertainty of less than 10%. For larger SZA the errors tend to become larger but are still generally less than 20% for SZA < 90°.

[38] For observations where the UVA transmission is less than 0.8, it is assumed that the radiation field is totally diffuse ($D = 1$) rather than as described by a radiative transfer model for clear skies. The use of this additional information, which is always available from a well-calibrated spectrometer measuring UV irradiances, results in significant improvements in accuracy of the conversion.

[39] Under cloudy conditions, errors at this site are generally less than 20% in the case of $J(O_3)$ but can be systematically larger in the case of $J(NO_2)$. A significant component of the error seems to be associated with departures in isotropy of skylight caused by the clouds rather than in calculating the diffuse fraction. However, this may not be the case at other more polluted sites, or when snow cover is present.

[40] In the absence of true actinic data, photolysis frequencies may be estimated, under the conditions encountered during the IPMMI campaign, from irradiance data. However, several assumptions are necessary, which may not generally be valid. If daily doses are sought, then very simple empirical relationships can be used, once the parameters have been established for the observing conditions.

[41] If photolysis frequencies are required for larger SZA, the conversion factors need to be determined using radiative transfer models. When this is done, there is a near-linear relationship between the derived fluxes and those directly measured over a wide range of observing conditions.

[42] Although changing cloud cover can have a large effect, there is a tendency for clouds to alter the clear-sky corrections systematically, resulting in deduced values of $J(NO_2)$ that are too large by ~10–20%. However, these systematic errors are smaller for $J(O_3)$.

[43] The conversion factors from irradiance to actinic fluxes are dependent on many variables including SZA, aerosol optical depth, cloud cover, and so on. Further study is needed to determine the errors involved in converting from irradiance to actinic flux under polluted conditions. Although the uncertainties in converting from irradiance to actinic fluxes may be large, the data may still be of sufficient quality to investigate differences in photolysis frequencies between sites where differences in UV irradiances are large [*Seckmeyer et al.*, 1995]. Under twilight conditions, when photolysis frequencies are in any case very low, it is not practicable to use irradiance data to obtain actinic fluxes.

[44] This study demonstrates that the potential exists to use the longer historical records and greater geographical coverage available from ground-based spectroradiometers measuring spectral irradiances to extend the database of photolysis frequencies at the surface.

[45] **Acknowledgments.** We gratefully acknowledge the contribution of Barry Bodhaine NOAA CMDL and Patrick Disterhoft of NOAA CIRES for providing on-site calibrations for the NIWA instrument. The National Center for Atmospheric Research is sponsored by the National Science Foundation. The FZJ part of this work received support by the German Federal Ministry for Education, Science, and Research (BMBF), grant 422-4007-07 TFS 30/B.2. The NIWA component of this work was carried out as part of contract CO1X0033 to New Zealand's Foundation for Research Science and Technology.

References

Blumthaler, M., J. Gröbner, M. Huber, and W. Ambach, Measuring spectral and spatial variations of UVA and UVB sky radiance, *Geophys. Res. Lett.*, *23*, 547–550, 1996.

DeMore, W. B., S. P. Sander, C. J. Howard, A. R. Ravishankara, D. M. Golden, C. E. Kolb, R. F. Hampson, M. J. Kurylo, and M. J. Molina, Chemical kinetics and photochemical data for use in stratospheric modeling: Evaluation number 12, *Rep. 97-4*, NASA Panel for Data Eval., Pasadena, Calif., 1997.

Harder, J. W., J. W. Brault, P. V. Johnston, and G. H. Mount, Temperature dependent NO_2 cross sections at high spectral resolution, *J. Geophys. Res.*, *102*, 3861–3879, 1997.

Herman, J. R., R. L. McKenzie, S. B. Diaz, J. B. Kerr, S. Madronich, and G. Seckmeyer, Ultraviolet radiation at the Earth's surface, in *UNEP/WMO Scientific Assessment of the Ozone Layer: 1998*, *44*, edited by D. L. Albritton et al., pp. 9.1–9.46, Global Ozone Res. and Monit. Proj., World Meteorol. Organ., Geneva, 1999.

Hofzumahaus, A., A. Kraus, and M. Müller, Solar actinic flux spectroradiometry: A new technique to measure photolysis frequencies in the atmosphere, *Appl. Opt.*, *38*(21), 4443–4460, 1999.

Kazadzis, S., A. F. Bais, D. Balis, C. S. Zerefos, and M. Blumthaler, Retrieval of downwelling UV actinic flux density spectra from spectral measurements of global and direct solar UV irradiance, *J. Geophys. Res.*, *105*, 4857–4864, 2000.

Madronich, S., Intercomparison of NO_2 photodissociation and UV radiometer measurements, *Atmos. Environ.*, *21*, 569–578, 1987.

McKenzie, R. L., P. V. Johnston, M. Kotkamp, A. Bittar, and J. D. Hamlin, Solar ultraviolet spectroradiometry in New Zealand: Instrumentation and sample results from 1990, *Appl. Opt.*, *31*, 6501–6509, 1992.

McKenzie, R. L., K. J. Paulin, G. E. Bodeker, J. B. Liley, and A. P. Sturman, Cloud cover measured by satellite and from the ground: Relationship to UV radiation at the surface, *Int. J. Rem. Sens.*, *19*, 2969–2985, 1998.

Molina, L. T., and M. J. Molina, Absolute absorption cross-sections of ozone in the 185 to 350 nm wavelength range, *J. Geophys. Res.*, *91*, 14,501–14,508, 1986.

Nader, J. S., and N. White, Volumetric measurement of ultraviolet energy in an urban atmosphere, *Environ. Sci. Technol.*, *3*, 849–854, 1969.

Ruggaber, A., R. Forkel, and R. Dlugi, Spectral actinic flux and its relationship to spectral irradiance by radiation transfer calculations, *J. Geophys. Res.*, *98*, 1151–1162, 1993.

Seckmeyer, G., et al., Geographical differences in the UV measured by intercompared spectroradiometers, *Geophys. Res. Lett.*, *22*, 1889–1892, 1995.

Shetter, R. E., and M. Müller, Photolysis frequency measurements using actinic flux spectroradiometery during the PEM-Tropics Mission: Instrument description and some results, *J. Geophys. Res.*, *104*, 5647–5662, 1999.

Stamnes, K., J. Slusser, and M. Bowen, Derivation of total ozone abundance and cloud effects from spectral irradiance measurements, *Appl. Opt.*, *30*, 4418–4426, 1991.

Van Weele, M., J. V.-G. D. Arellano, and F. Kuik, Combined measurements of UVA actinic flux, UVA irradiance and global radiation in relation to photodissociation rates, *Tellus*, *47B*, 353–364, 1995.

Zeng, J., R. McKenzie, K. Stamnes, M. Wineland, and J. Rosen, Measured UV spectra compared with discrete ordinate method simulations, *J. Geophys. Res.*, *99*, 23,019–23,030, 1994.

J. Calvert, C. Cantrell, S. Mandronich, and R. Shetter, National Center for Atmospheric Research, 1850 Table Mesa Drive, Boulder, CO 80303, USA. (calvert@acd.ucar.edu; cantrell@ncar.ucar.edu; sasha@acd.ucar.edu; shetter@ucar.edu)

A. Hofzumahaus, Institut für Atmosphärische Chemie und Dynamik der Geosphäre, ICG-3/AH, Forschungszentrum Jülich, Postfach 1913, D-52425 Jülich, Germany. (a.hofzumahaus@fz-juelich.de)

P. Johnston and R. McKenzie, National Institute of Water and Atmospheric Research, Private Bag 50061, Omakau, Central Otago, New Zealand. (p.johnston@niwa.cri.nz; r.mckenzie@niwa.cri.nz)

A. Kraus, Department of Pharmacokinetics, Research and Development, Grünenthal GmbH, Zieglerstr. 6, D-52078 Aachen, Germany. (alexander.kraus@grunenthal.de)